nature water

Article

https://doi.org/10.1038/s44221-023-00103-7

MOF water harvester produces water from Death Valley desert air in ambient sunlight

Received: 14 December 2022

Accepted: 5 June 2023

Published online: 06 July 2023

Check for updates

Woochul Song[1,2,3,4], Zhiling Zheng[1,2,3], Ali H. Alawadhi[1,2,3] & Omar M. Yaghi[1,2,3]

Sorbent-assisted atmospheric water harvesting has emerged as a promising method to mitigate water stresses in arid climates. Here a new water harvester based on metal–organic frameworks (MOFs) has been designed, constructed and tested in two locations in California (Death Valley National Park and Berkeley). This water harvester is capable of harvesting water at a capacity of 210 and 285 g H_2O per kilogram of MOF-303 per day, respectively. The unique configuration of the MOF cartridge and the condenser in the harvester allows the highest efficiency of water uptake and harvesting from air without power or energy input aside from ambient sunlight. Indeed, this water harvester operates passively with double the amount of water harvested compared with our previous passive MOF water harvester. These results highlight the great potential for addressing the water stress problem in the world.

Although access to water is recognized as a fundamental human right, over five billion people are expected to experience water stress by the year 2050 (refs. 1–3). Climate change is exacerbating this problem by causing severe droughts and therefore affecting the lives and livelihoods of large segments of the world population[4,5]. Water desalination offers a solution, but it is important to develop off-grid water supply technology to close the gap between the regions that cannot receive the benefits from the centralized water supply infrastructures. Given that there is almost as much water in the atmosphere at any given time as there is in lakes and rivers on our planet, the question of whether this water could be harvested in an energy-efficient manner is foundational to solving the water scarcity problem[6–8]. In this article, we report the design and construction of a device into which a metal–organic framework (MOF) material has been integrated in a form to maximally expose it to air and allow the extraction of water at night and its collection during the day when exposed to ambient sunlight. This MOF water harvester was demonstrated in the Death Valley desert air in the month of August 2022 demonstrating the ability to collect 114–210 g H_2O per kilogram of MOF per day under ambient temperature swing of 21.9–60.7 °C between night and day with a relative humidity (RH) ranging from 9.4% to 36%. No other water harvesting system has been reported to operate under such extreme conditions and without energy input aside from ambient sunlight.

Others and we have developed atmospheric water harvesting (AWH) based on MOFs[9–11], porous polymers[12], zeolites[13] and other porous or hygroscopic materials[14–17]. Harvesters based on these have been tested either in the laboratory[11,17], the field or both[9,10,12–16] with power supply (that is active). Only one system using ambient sunlight with no other source of energy or power (that is passive) has been tested in the desert (Fig. 1a)[18]. Our current MOF water harvester collected double (2.06-fold higher) the amount of water per kilogram of MOF (grams H_2O per kilogram of MOF) under even more extreme conditions in the Death Valley (as indicated by the red arrow in Fig. 1b). In particular, the device was loaded with MOF-303 (Al(OH)(PZDC); PZDC, 1*H*-pyrazole-3,5-dicarboxylate), of which water isotherm has the water uptake inflection point at 12% RH with uptake capacity of 39 wt% at 20% RH[9,18–20].

This new-generation MOF water harvester reported here was developed focusing on the following criteria: (1) increasing the volume-to-surface area ratio (VS-r) of MOF bed, (2) designing MOF bed assembly (MOF cartridge) to efficiently distribute heat under the solar irradiance and (3) optimizing the condenser to accelerate the condensation rates. Each step is responsible for effective water sorption, desorption and

[1]Department of Chemistry, University of California, Berkeley, CA, USA. [2]Kavli Energy Nanoscience Institute, University of California, Berkeley, CA, USA. [3]Bakar Institute of Digital Materials for the Planet, College of Computing, Data Science, and Society, University of California, Berkeley, CA, USA. [4]Present address: Division of Environmental Science and Engineering, Pohang University of Science and Technology (POSTECH), Pohang, South Korea. e-mail: yaghi@berkeley.edu

https://doi.org/10.1038/s44221-023-00103-7

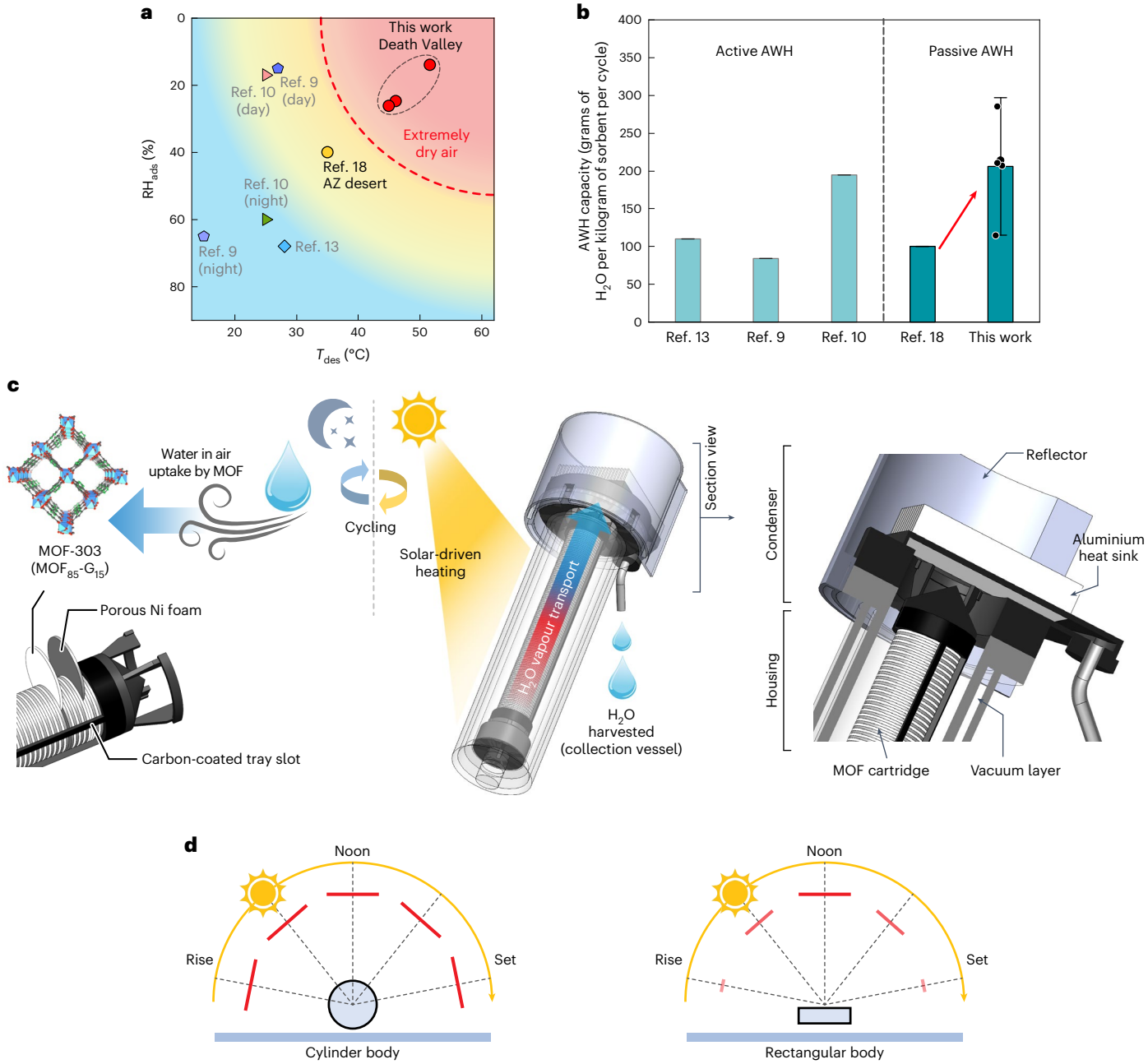

Fig. 1 | New generation of passive MOF water harvester. a, Operational conditions of representative MOF[9,10,18]- and zeolite[13]-based water harvesters tested in the field. Only one passive water harvester was tested in the field (Arizona, AZ, desert). RH_{ads} (%): RH during sorption cycle. T_{des} (°C): average ambient temperature during desorption cycle. **b**, AWH capacity per one harvesting cycle. For refs. 9 and [10], average values during the day and the night were used. For this work, average value of five field test results in both Berkeley and the Death Valley is used. Data are presented as mean ± standard deviation ($n = 5$). **c**, General configuration of the MOF water harvester. At night, MOF cartridge is exposed to air to capture atmospheric water. During the day, the MOF cartridge is assembled into the vacuum-insulated device housing and condenser. Upon the solar irradiance, water is released from MOF by solar-driven heating and transported to the condenser. Direct solar irradiance to the condenser is shielded by reflector, and water is condensed at the surface of aluminium heat sinks. Condensed water is collected into the collection vessel connected to the condenser by the tube. **d**, Schematic illustration showing the projected area differences (red lines) between cylindrical and rectangular shape bodies from sunrise to sunset.

condensation that are critical for efficient and practical AWH but have not been systemically investigated in this field. In addition, the MOF cartridge was designed to have constant VS-r irrespective of the MOF amounts used in the device, an aspect that improves its scalability. As a result of this systematic investigation, the present harvester enabled completely passive AWH even under the extremely dry and hot air conditions in the Death Valley where the highest ambient temperature near the ground was 60 °C and the lowest average RH (RH_{avg}) of the nights was 14% during our field tests.

Construction of passive MOF water harvester

The device was designed to have two main compartments (Fig. 1c and Supplementary Figs. 1–8). One is the housing for the MOF cartridge, and the other is the condenser. The transparent cylinder-shape housing included vacuum insulated double-wall structure to prevent conductive heat loss to environments under solar irradiation. Also, compared with the rectangular geometry that other devices used[13,18,21], the cylinder-shaped module can maximize the use of solar energy from the sunrise to sunset since the projected area of

https://doi.org/10.1038/s44221-023-00103-7

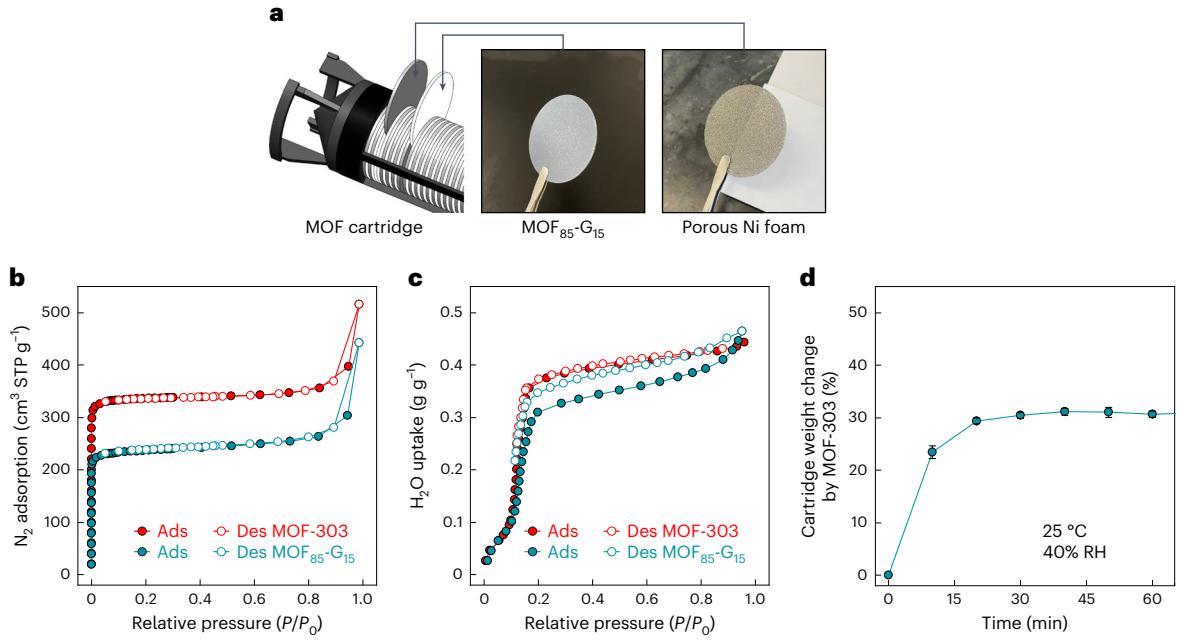

Fig. 2 | MOF cartridge design and water uptake properties. a, Photographs of the MOF cartridge, MOF_{85}-G_{15} pellet and porous Ni foam disc. **b**, N_2 isotherm of MOF-303 and MOF_{85}-G_{15} pellet at 77 K (Ads: adsorption, Des: desorption). **c**, Water isotherm of MOF-303 and MOF_{85}-G_{15} pellet at 25 °C. **d**, Weight change of the MOF cartridge at 25 °C and 40% RH. The weight change is presented normalized to the MOF-303 weight (35 g). Data are presented as mean ± standard deviation (n = 3).

the cylinder body towards the sun is consistent alongside the sun trajectory (Fig. 1d).

The condenser components are located on the top of the housing to utilize the air density (temperature) gradients inside the device as a driving force of convective vapour transport from the MOFs to the condenser. In principle, the MOF cartridge and condenser require different thermal conditions to improve AWH during the day. The cartridge needs to be heated for water desorption and the condenser cooled down for condensation, respectively. Therefore, by placing the condenser on top and separating these two compartments, such contradictive conditions could be balanced and optimized in way reminiscent of rotary evaporator commonly used in chemistry laboratories. Also, since the condenser is facing clear sky, we can expect the potential device design that use radiative energy dissipation to further accelerate water condensation[22,23].

MOF cartridge design and assembly

For efficient AWH, it is important to maximize the exposure of MOFs to external air during both adsorption and desorption steps. For example, in our former study that used MOF-801, as the VS-r of MOF beds decreases from 1 to 0.5, water uptake capacity decreased from 230 to 210 g H_2O per kilogram of MOF-801 due to the reduced accessibility of MOFs to the air, resulting in the reduced AWH capacity from 130 to 56 g H_2O per kilogram of MOF-801 per day[18]. Therefore, in this work, MOF powders were processed into the thin disc-shaped pellets (38 mm in diameter and ~0.8 mm in height), and these pellets are stacked with porous nickel (Ni) foam discs (38 mm in diameter and 1.5 mm in height) to maintain VS-r of 2.6 (Figs. 1c and 2a). Since the porosity of the Ni foam is higher than 97%, the external air can flow and diffuse through this porous structure, making the MOF pellet surfaces exposed to the air. Also, Ni foam has ~90 W m^{-1} K^{-1} thermal conductivity and can serve as heat conductor in between MOF pellets under the solar irradiation, which is also important as the MOFs are typically thermal insulators with a conductivity of less than 2 W m^{-1} K^{-1} (refs. 24–27).

Sorbent pellets were prepared by mixing the activated MOF-303 powders with graphite in different weight ratios and uniaxially pressing them under the pressure of 78 MPa for 2 min (Supplementary Figs. 9–14). Graphite was introduced as a binder to improve both the mechanical property and the thermal conductivity of the pressed bodies, and the pellets prepared using 85 wt% MOF-303 and 15 wt% graphite (MOF_{85}-G_{15}) were further used for the device fabrication. The N_2 BET surface area of MOF_{85}-G_{15} is 955 m^2 per gram of MOF_{85}-G_{15}, which corresponds to 1,120 m^2 per gram of MOF-303, showing that more than 85% of MOF-303 surface area (1,370 m^2 g^{-1}) was preserved under the pressing process (Fig. 2b). Also, MOF_{85}-G_{15} pellets showed the characteristic water isotherm profile of MOF-303 that has the inflection point at ~12% RH, while having water uptake capacity of 29 wt% by MOF_{85}-G_{15} (35 wt% by MOF-303) at 20% RH, which also corresponds to the 85% capacity of MOF-303 (Fig. 2c). It is noteworthy that hydrophobic graphite binder was also advantageous in enhancing water resistance of the pressed pellets. When hydrophilic cellulose binders were used, the pellets were immediately dissociated in water while MOF_{85}-G_{15} maintained their shapes more than 24 h, showing the enhanced water resistance (Supplementary Fig. 15).

Water uptake properties of the entire MOF cartridge assembly were investigated. The cartridge was activated in an oven at 140 °C for 24 h, and the net weight change of the cartridge was measured at 25 °C and 40% RH in the environmental chamber. When 35 g MOF-303 was used (42 g of MOF_{85}-G_{15}), ~32 wt% increase was observed within 2 h, showing that more than 90% of the MOF-303 in MOF_{85}-G_{15} was accessed (Fig. 2d). Also, the same uptake efficiencies were observed when 25 g and 45 g of MOF-303 were used, respectively (Supplementary Fig. 16). This implies that atmospheric air accessibility is maintained regardless of the amount of MOFs used. This is due to the constant VS-r resulting from the stacking configuration of MOF_{85}-G_{15} pellets and porous Ni foam discs. As a result, water uptake efficiency will not be affected even at more than kilogram scale, showing the great potential for scalability.

Heat and energy transfer simulation under solar irradiance

Before the device fabrication, heat and energy transfer under solar irradiation was investigated using computer simulations. Equations of radiative, convective, and conductive heat and energy transfer were integrated for the simulations. Note that heat of water desorption

https://doi.org/10.1038/s44221-023-00103-7

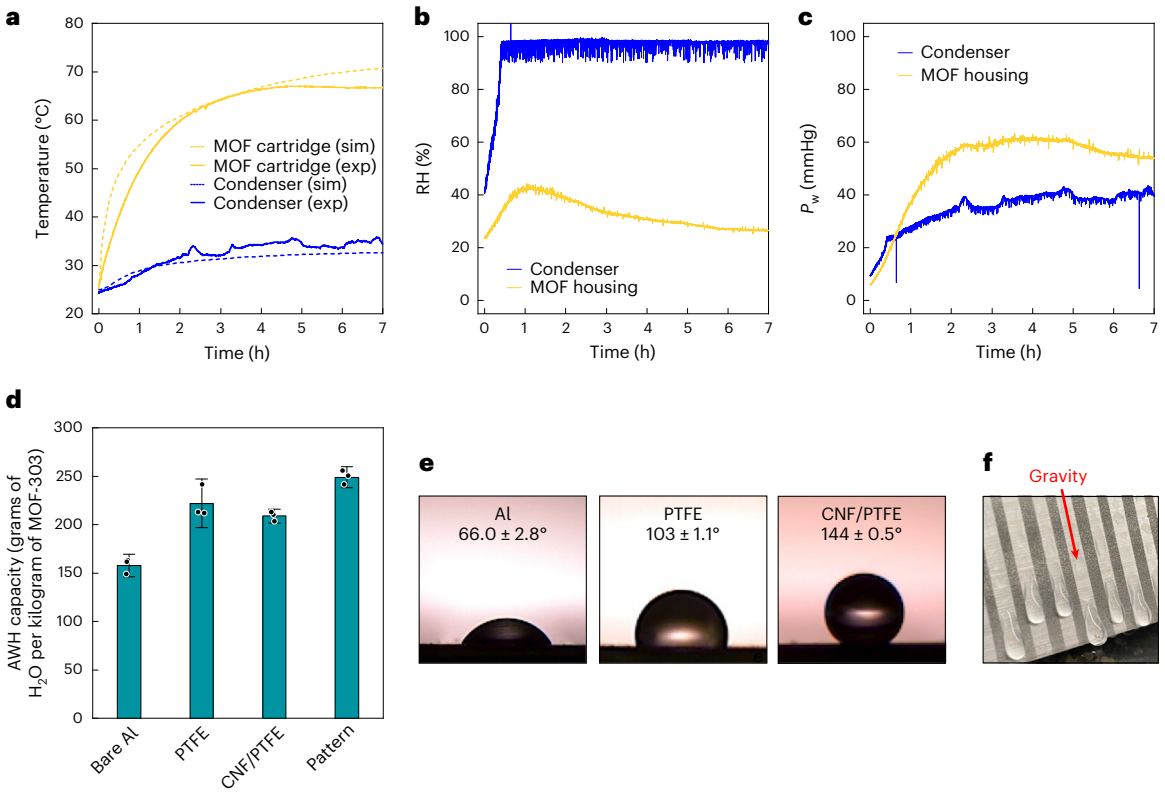

Fig. 3 | Laboratory test of the passive AWH device. a, Simulated (sim) and experimental (exp) temperature change of the MOF cartridge and condenser under light irradiance. **b**,**c**, Experimental RH (**b**) and P_w (mmHg) (**c**) change of the MOF housing and condenser during the laboratory test. **d**, AWH capacity of the device tested with different surface conditions of the condensers, which are bare aluminium (Al, non-treated), PTFE coated, CNF/PTFE coated and patterned coating with CNF/PTFE. Data are presented as mean ± standard deviation ($n = 3$). **e**, Water–air interface contact angle measurements of bare (Al), PTFE- and CNF/PTFE-coated condensers. **f**, Photograph of the condenser surface with linear patterned CNF/PTFE coating (black strips) alongside the direction of gravity.

from MOF_{85}-G_{15} and latent heat release by water condensation are not considered in this computational study. As a result, under the solar irradiance of 1,000 W m^{-2} for 7 h, the MOF bed temperature increases up to 70 °C (Fig. 3a and Supplementary Fig. 17) and no greater than 2 °C temperature differences were observed over the MOF pellet stacks, showing the effective heat distribution by the cartridge design. Also, 10 °C temperature difference of MOF was observed between non-insulated single and vacuum-insulated double-wall MOF housing structures. Importantly, the temperature difference between the cartridge and the condenser was maintained greater than 35 °C after 7 h (Fig. 3a), showing the successful heat dissipation to environments through heat sinks and therefore the potential for water condensation.

Laboratory test of the passive water harvester

Based on the results of MOF cartridge water uptake experiments and energy transfer simulations, the entire device was fabricated and tested in the laboratory. First, the activated cartridge with 35 g MOF-303 (42 g MOF_{85}-G_{15}) was exposed to the 20 °C and 35% RH air for 8 h in the environmental chamber. After this water uptake step, the cartridge was assembled and the device was exposed to 4,000 K light (950 W m^{-2}) for 7 h monitoring of the temperature, RH and water vapour pressure (P_w, mmHg) changes at different points of the device (Fig. 3a–c). Upon the light irradiance, the temperature of the MOF_{85}-G_{15} in the cartridge started to increase instantly, reaching to the highest temperature of 67 °C. The temperature profiles of experiments and simulations showed good correspondence with each other (Fig. 3a), while the MOF temperature increases less rapidly than the simulation at the initial stage and the condenser temperature is slightly high. This could be attributed to the heat of water desorption and condensation at the MOF bed and the condenser, respectively, which were not considered in the simulations. Importantly, spatial RH change in the device evidently showed the vapour transport from the MOF cartridge to the condenser. RH at the condenser gradually increased after the device was exposed to the light and reached to 100% within 1 h (Fig. 3b,c). On the other hand, the RH near the cartridge initially increased and then decreased as water is condensed and collected, showing the water transport from the MOF_{85}-G_{15} to the inner space of the housing, condenser, and finally collection vessel. As a result, 5.5 (±0.27) g water was harvested, achieving the AWH capacity of 157 (±7.8) g H_2O per kilogram of MOF-303 (Fig. 3d). Mass change of MOF-303 during the experiments is summarized in Supplementary Table 1.

Condenser surface modification for facile water condensation

Since water condensation is a key step, we further investigated this effect to improve the AWH capacity. One general strategy to improve the condensation rate is to modify the surface as hydrophobic for dropwise condensations[28] (Supplementary Fig. 6). We first tried polytetrafluoroethylene (PTFE) and carbon nanofibre–PTFE composites (CNF/PTFE) materials for hydrophobic surface treatments, using a reported spray-coating method[29]. The hydrophobicity increased in the order of bare aluminium (Al, non-treated condenser surface) to PTFE- to CNF/PTFE-coated surfaces as confirmed by the water–air interface contact angles that are 66° (±2.8°), 103° (±1.1°) and 144° (±0.5°), respectively (Fig. 3e). The AWH capacity increased from 157 (±7.8) (Al) to 220 (±16) (PTFE coating) and 210 (±4.7) g H_2O per kilogram of MOF-303 (CNF/PTFE coating) (Fig. 3d and Supplementary Fig. 18).

https://doi.org/10.1038/s44221-023-00103-7

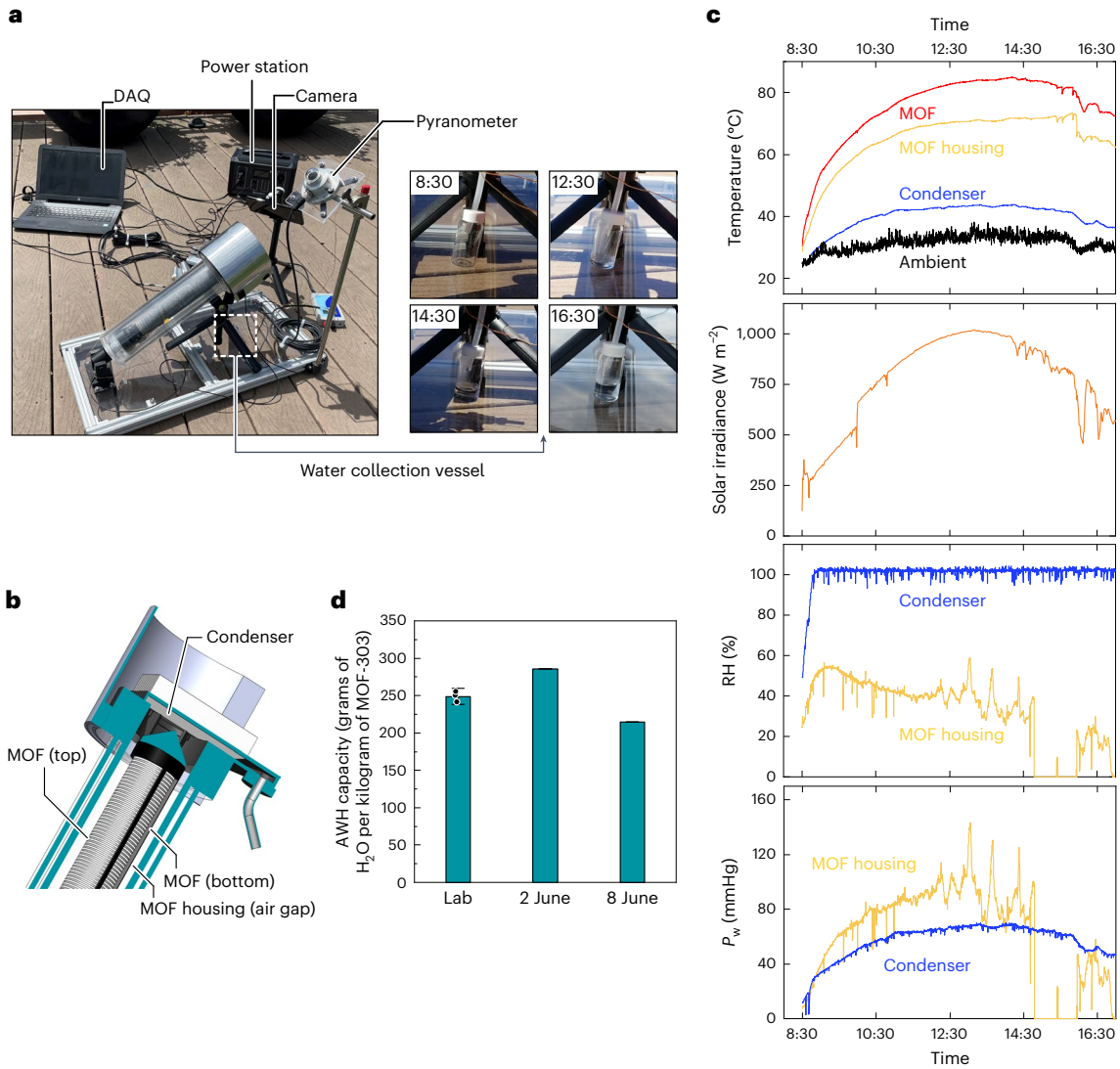

Fig. 4 | AWH in Berkeley. a, Photographs of the device setup including power station (500 Wh), pyranometer and data acquisition (DAQ) systems, and water collected at different times during the 10 June test. **b**, Sectional drawing of the device to show the different measurement points of temperature and RH. Sectional plane caps are coloured with turquoise for visual clarity. **c**, Temperature (°C), solar irradiance (W m^{-2}), RH (%) and P_w (mmHg) changes of the device and ambient air conditions during the 10 June test. Time axes are synced with each other. **d**, Comparison of AWH capacity between the lab and Berkeley field test conditions. Data are presented as mean ± standard deviation ($n = 3$).

While the capacity improved once the surfaces were modified, no substantial difference between PTFE- and CNF/PTFE-coated condensers was observed. We hypothesized that, as the hydrophobicity of the condensation surface becomes greater, the water nucleation step becomes more important in determining the condensation rates, especially for the passive AWH. For example, condensation takes place as a serial step of nucleation, growth, droplet coalescence and water removal by gravity[28]. In many applications, dropwise condensation by hydrophobic surfaces is preferred since it removes the coalesced droplets quickly by gravity to minimize surface wetting that function as additional resistance for continued condensation. This implies that the nucleation step is less critical in determining the rates, which prefer hydrophilic surfaces with high surface energy[30]. However, we believed that this initial step could be more critical in the passive AWH applications. Since the vapour is transported to the condenser under much milder conditions compared with the other applications such as hot steam generation plants[31], there would be less gradients to drive one-directional vapour–liquid phase changes initiated by nucleation[32]. Therefore, since the nucleation step could be important in the present case, we introduced the strip-pattern CNF/PTFE coatings on the surface alongside the direction of gravity (Fig. 3f). This is to promote initial water nucleation and growth of coalesced water droplets in the hydrophilic channels, and then remove merged water by gravity rather than let water adhere over the entire metal contact due to the high surface energy (Fig. 3f). As a result, when the hydrophobic strip pattern was introduced to the condenser surface, the first droplet of the harvested water in collection vessel was observed within 1.5 h, which is 45 min faster than the other conditions, supporting that the patterned coating could accelerate the condensation rates. Also, the AWH capacity increased from 210 (±4.7) to 248 (±7.2) g H_2O per kilogram of MOF-303 (Fig. 3d).

Water harvesting in the field: Berkeley, CA, United States

Our passive water harvester was tested outdoors in Berkeley on two different days, when the average ambient temperature (T_{avg}) during the day cycle was relatively higher (2 June 2022) and lower (10 June 2022) than the indoor laboratory conditions (25 °C) (Fig. 4a, Supplementary Fig. 19 and Supplementary Table 2). The T_{avg} and the average solar irradiance intensity (I_{avg}) were 19.6 °C and 620 W m^{-2}, and 31.5 °C and

https://doi.org/10.1038/s44221-023-00103-7

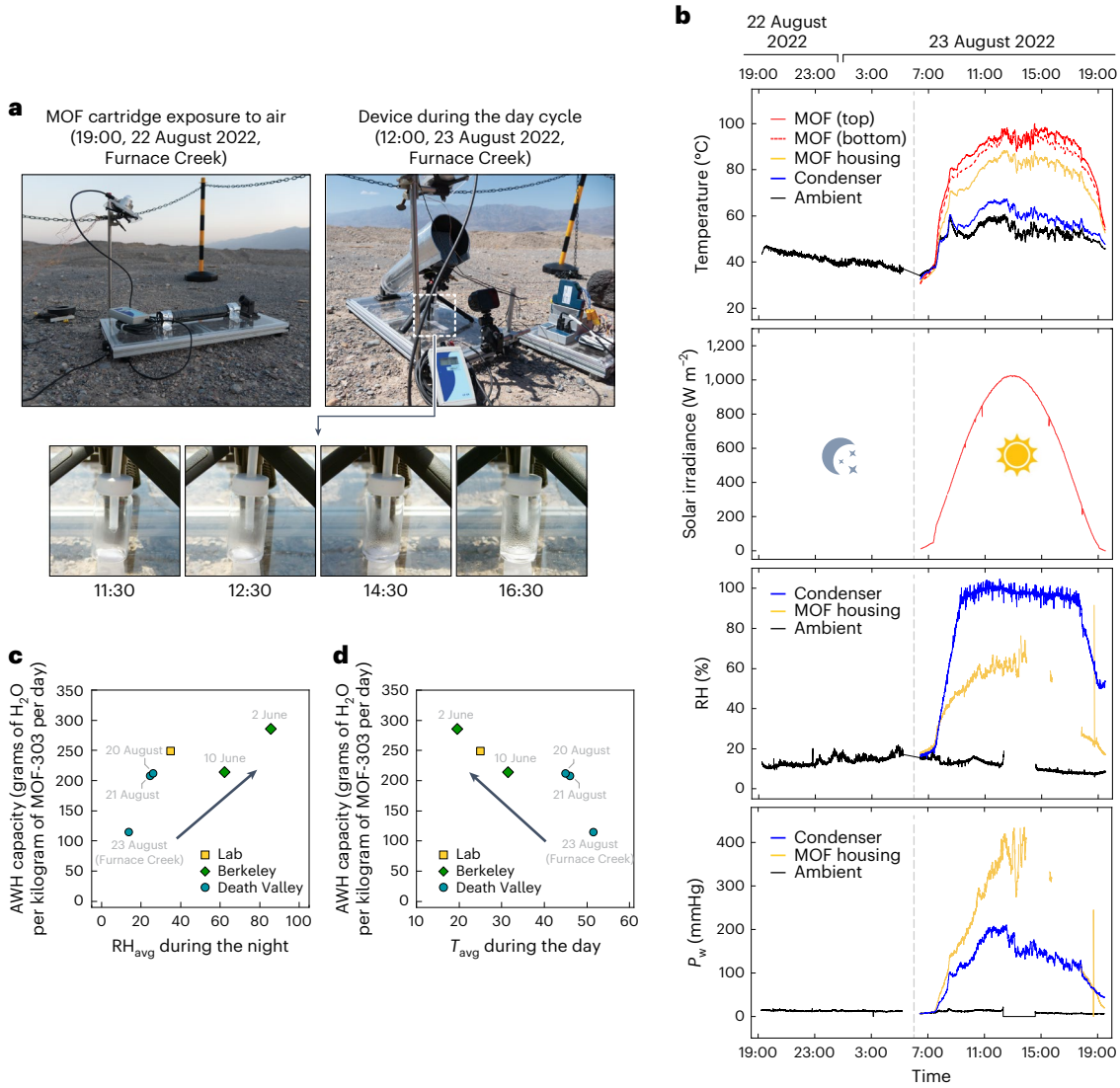

Fig. 5 | AWH in the Death Valley. a, Photographs of the AWH at Furnace Creek, showing the MOF cartridge exposed to air for water uptake (top left), the device during the day cycle (top right), and water collected at different time (bottom). **b**, Temperature (°C), solar irradiance (W m^{-2}), RH (%) and P_w (mmHg) changes of the device and ambient air conditions during the 23 August test. Time axes are synced with each other. **c**,**d**, AWH capacity as a function of RH_{avg} (**c**) and T_{avg} (**d**) during the night and day cycles, respectively.

720 W m^{-2}, respectively. During the night cycles, the activated MOF cartridge was left outdoor, and the day cycle tests were performed for 8 h from 8:30 to 16:30 monitoring the temperature, RH and solar irradiance (Fig. 4b,c).

Upon the exposure to sunlight, the spatial temperature and RH of the device changed with the similar profiles observed in the laboratory tests (Figs. 3a and 4c) and the device successfully harvested water on both days, achieving AWH capacity of 285 and 210 g H_2O per kilogram of MOF-303 per day on 2 June and 10 June, respectively (Fig. 4d). The 2 June result showed even higher water productivity than the indoor laboratory tests, which could be attributed to improved condensation owing to the lower ambient temperature and therefore more efficient both conductive and convective (by outdoor airflow) heat release to the atmosphere. In addition, during the 10 June test, the condenser temperature increased up to 43 °C, notably higher than the temperature observed in the laboratory, but water was successfully harvested.

The fact that, in our previous study that tested the previous version of passive device in Arizona (AZ) desert, condensation was not observed at a similar condenser (42 °C) and atmosphere (35 °C of the peak during the day cycle) temperature conditions[18] indicated the importance of the following design considerations for the passive AWH device: (1) choosing condenser materials with good wettability to attract water molecules for surface adhesion since the previous device used poly(methyl methacrylate) plastics as the condenser and (2) guiding humid air into the confined space so that the air condition reaches to the dew point (100% RH) and maintain this condition effectively, an aspect driven by air density differences between the housing and the condenser in this study (Fig. 1c).

Water harvesting in the field: Death Valley, NV and CA, United States

The device was further tested in the Death Valley areas in mid-summer during the month of August 2022, to assess the AWH even under extremely dry and hot air conditions. The tests were performed for full three night-and-day cycles, namely two cycles near the east boundary of the Death Valley National Park (36.5319° N, −116.5455° W) from 19 August to 21 August 2022 and another cycle at the Furnace Creek (36.4506° N, −116.8523° W) from 22 August to 23 August 2022, the latter

https://doi.org/10.1038/s44221-023-00103-7

Table 1 | $SY_{water,max}$, η and the other parameters required for the calculation

	T_{des}[a] (°C)	T_{amb}[a] (°C)	RH_{avg} (%)	P_{total}[b] (Wh)	L_{max}[b] ($ml\,h^{-1}$)	$SY_{water,max}$ ($lkW^{-1}h^{-1}$)	η (%)
Berkeley 2 June	56.1	19.6	86	1.59	1.88	1.18	66.4%
Berkeley 9 June	65.1	31.5	62	1.40	1.66	1.29	56.4%
Death Valley 19 August	64.6	46.5	24.8	0.78	0.95	1.21	60.0%
Death Valley 20 August	70.9	45.0	26.2	0.77	0.92	1.20	60.2%
Death Valley 22 August	79.8	51.6	14	0.61	0.73	1.20	41.9%

[a]Average desorption (des) and ambient (amb) temperatures during the day cycles. [b]L_{max} and P_{total} are maximum water production rate during the day cycle and total energy required to desorb all water molecules from adsorbents, respectively.

being the driest location of the Death Valley due to the elevation below sea level at the centre of the valley (Fig. 5a, Supplementary Figs. 20–24, Supplementary Table 2 and Supplementary Videos 1–3).

During these tests, the lowest daytime peak temperature near the ground was 56 °C (21 August) and the highest nighttime RH_{avg} was 26%. Especially in the Furnace Creek location, the RH_{avg} during the night was just 14% with a peak of 21% at around 4:30 (Fig. 5b). Even under this extreme weather condition that the condenser temperature reached to 65 °C, the device successfully harvested water from air with the AWH capacity of 114 g H_2O per kilogram of MOF-303 per day. Considering all these tests, the highest productivity of the device was 210 g H_2O per kilogram of MOF-303 per day in the Death Valley area. For comparison, the AWH capacities are summarized in Fig. 5c,d as a function of RH_{avg} and T_{avg} during the night and day cycles, respectively. Strong relationships are evident between these two factors and AWH capacity, confirming that both humidity and temperature conditions are critical in determining the efficiency of passive MOF harvesting. These results also emphasize again the importance of condensation process to improve passive water harvesting capacity. These aspects have not been considered as much as other factors such as sorbents' intrinsic water uptake properties or the sorbent bed structures.

To provide thermodynamic analysis of this passive device, maximum specific yield of water ($SY_{water,max}$) and the device efficiency (η) are calculated for each field test results (Table 1). $SY_{water,max}$ ($l\,kWh^{-1}\,h^{-1}$) is maximum amount of water that can be extracted from air at given test conditions, while η (%) shows the actual performance efficiency of the device compared with $SY_{water,max}$ (Supplementary Methods gives the analysis details). Compared with the other reported systems that potentially have η between approximately 10% and 35% (ref. 6), this device showed η of ~41–66% even at extreme weather conditions (Table 1). In principle, even though direct comparison of different passive AWH systems is not appropriate as the key parameters for the calculation such as test conditions (for example, desorption temperature, ambient temperature and RH) and isosteric heat of sorption are different, it still shows the greatest potential of our device to enable practical passive AWH.

Summary

A passive water harvester based on MOF-303 has been designed and configured to achieve the highest efficiency among passive designs. A water harvesting capacity of 285 g H_2O per kilogram of MOF-303 per day with only ambient sunlight and no power or other energy input was achieved. The MOF cartridge design and the condenser surface treatments were key features in achieving high water harvesting efficiency especially when tested in the field (Death Valley National Park). Also, the capacity per unit area is important for passive operations to minimize environmental footprint. In this regard, owing to the compact and modular design, water productivity of 200 g of H_2O per m^2 per day was achieved, which is three folds higher than our previous device (65 g of H_2O per m^2 per day)[18]. While our new passive device shows great potential in harvesting atmospheric water, there are also challenges to be addressed to deliver the impacts of this technology into global communities. First, even though this passive device can harvest water from air without any cost, energy and carbon emission to environments once they are installed, further economic and environmental assessments need to be performed including the processes of both device fabrication and MOF synthesis. For example, we recently proposed green and scalable methods of MOF-303 synthesis[33], but the assessments have not been performed regarding with economic and environmental impacts that are involved in the preparation of MOF building blocks (metal salts and organic linkers) and activation solvents. In addition, to draw a meaningful cost–benefit analysis, these factors would need to be coupled with long-term cycling performance of the scalable passive systems so that accurate techno-economic values can be compared with the existing water supply systems. In this perspective, passive AWH systems are still in earlier stage compared with the active systems[6,7,34]. Therefore, for future research, it will be important to provide any relevant data such as isosteric heat of sorption and detailed field test conditions to carry out such analyses, in addition to improving AWH capacity by materials developments as well as device design and optimizations.

Methods

Details of the experimental methods that are not described in this section are available in Supplementary Information.

MOF-303 synthesis and MOF_{85}-G_{15} preparation

MOF-303 was synthesized using the method previously reported[18]. In brief, 8.072 g (51.7 mmol) of 3,5-pyrazoledicarboxylic acid (H_2PZDC) was dissolved in 420 ml of de-ionized (DI) water slowly adding 30 ml of 2.6 M NaOH solution by stirring for 10 min. The solution was sonicated for 5 min. Then 12.5 g (51.7 mmol) of aluminium chloride hexahydrate ($AlCl_3{\cdot}6H_2O$) was added to the solution by stirring for 5 min and heated at 100 °C for 24 h. The precipitates were divided into 50 ml tubes and washed with DI water by centrifugation three times over the course of 24 h for 3 days, followed by washing with methanol over the course of 24 h for 3 days. The samples were air-dried for 24 h and activated at 150 °C either under the vacuum (for 10 h, powders) or in the convection oven (for 2 days, MOF pellets). For MOF_{85}-G_{15} preparation, the activated MOF-303 was mixed with 15 wt% graphite. The mixture was ground in mortar, and pressed using the bench top hydraulic press (Carver, 4350 model) with 38 mm circular-shaped press dye at a pressure of 78 MPa for 2 min.

Device design and fabrication

The device parts were designed using SOLIDWORKS 3D CAD software. The details of the part drawings with dimensions are available in Supplementary Information (Supplementary Figs. 4–7). The MOF housing was fabricated by co-centring two PMMA acrylic tubes with custom-made acrylic cap and flange using acrylic glue to form vacuum layer. One 1/8 FNPT threaded port was made on the outer tubing shell to be connected to vacuum pump, and the vacuum was hold using the valve during the test (Supplementary Fig. 4). The MOF cartridge tray slot was custom machined using Al tubing (38 mm inner diameter × 44 mm outer diameter) and coated with conductive carbon paint (MG Chemicals, 838AR) using a paint brush. The other parts of the device were 3D printed using Markforged Onyx One printer with micro-carbon-filled nylon (Onyx) filaments. Two aluminium heat sinks (40 mm × 100 mm × 20 mm) were used as the condenser.

PTFE and CNF/PTFE surface coating of the aluminium heat sinks

Hydrophobic coating of the Al condenser surfaces were conducted using the previously reported method[29]. In brief, for CNF/PTFE coating, 180 mg of PTFE powder (Sigma Aldrich, cat. no. 430935) and 20 mg of CNF (Sigma Aldrich, cat. no. 719781) was mixed with 20 g of dichloromethane and dispersed using the probe sonicator for 2 min. This CNF/PTFE/dichloromethane suspension was loaded in VL double-action airbrush (Paasche) and sprayed over the heat sink surfaces. The heat sink was heated at 400 °C for 30 min for CNT/PTFE annealing on the surface and then cooled down to room temperature. For PTFE coating, the same procedure was used except for using only CNF in preparing the suspension solution. For the patterned CNF/PTFE coating, the condenser surface was masked using 3-mm-thick masking tapes before spraying CNF/PTFE solution. The masking tapes were removed, and the condenser was annealed as described earlier.

Contact angle measurements

Water–air interface contact angles were measured using the custom-made measurement apparatus. Using the micropipette, 10 µl of DI water was placed on the subject surfaces and the droplet photographs were taken using the camera. The contact angles were analysed using the contact angle plug-in of ImageJ software.

Lab tests of the device

Before the tests, the MOF cartridge was activated in an oven at 140 °C for more than 16 h and incubated in the SH-242 ESPEC environmental test chamber with 20 °C and 35% RH air conditions for 8 h. After this, the cartridge was assembled into the device and exposed to 4,000 K light with 45° irradiation angle. Light intensity was adjusted to be 950 W m^{-2} using the Hukseflux LP02-C pyranometer connected to the LI-19 data logger. Each indoor test was carried out for 7 h, monitoring the temperature and RH changes of the MOF_{85}-G_{15}, the case (air gap between MOF cartridge and housing) and the condenser.

Field tests of the passive AWH device

The MOF cartridge was activated in an oven at 140 °C for more than 16 h. During the night cycles, the MOF cartridge was left outdoors overnight for atmospheric water uptake. For the day cycles, the cartridge was assembled, and the device was set facing the south pole to maximize the use of sunlight as described in Fig. 1d. The tests were carried out from 8:30 to 16:00 in Berkeley area and from sunset to sunrise in the Death Valley area, respectively (Supplementary Table 1), monitoring the temperature and RH changes. The exact locations of each test are followings: 2 June and 8 June 2022 (37.8715° N, 122.2730° W), from 19 August to 21 August 2022 (36.5319° N, −116.5455° W), and from 22 August to 23 August 2022 (36.4506° N, −116.8523° W).

Reporting summary

Further information on research design is available in the Nature Portfolio Reporting Summary linked to this article.

Data availability

The datasets that support this study are available in Zenodo repository with identifier (https://doi.org/10.5281/zenodo.7990951).

References

1. *The Sustainable Development Goals Report* (United Nations, 2018).
2. *State of Global Water Resources 2021* (World Meteorological Organization, 2022).
3. Mekonnen, M. M. & Hoekstra, A. Y. Four billion people facing severe water scarcity. *Sci. Adv.* **2**, e1500323 (2016).
4. Famiglietti, J. S. The global groundwater crisis. *Nat. Clim. Change* **4**, 945–948 (2014).
5. Hoekstra, A. Y. & Mekonnen, M. M. The water footprint of humanity. *Proc. Natl Acad. Sci. USA* **109**, 3232–3237 (2012).
6. Peeters, R., Vanderschaeghe, H., Rongé, J. & Martens, J. A. Energy performance and climate dependency of technologies for fresh water production from atmospheric water vapour. *Environ. Sci. Water Res. Technol.* **6**, 2016–2034 (2020).
7. Lord, J. et al. Global potential for harvesting drinking water from air using solar energy. *Nature* **598**, 611–617 (2021).
8. Lu, H. et al. Materials engineering for atmospheric water harvesting: progress and perspectives. *Adv. Mater.* **34**, 2110079 (2022).
9. Hanikel, N. et al. Rapid cycling and exceptional yield in a metal–organic framework water harvester. *ACS Cent. Sci.* **5**, 1699–1706 (2019).
10. Almassad, H. A., Abaza, R. I., Siwwan, L., Al-Maythalony, B. & Cordova, K. E. Environmentally adaptive MOF-based device enables continuous self-optimizing atmospheric water harvesting. *Nat. Commun.* **13**, 4873 (2022).
11. Kim, H. et al. Water harvesting from air with metal–organic frameworks powered by natural sunlight. *Science* **356**, 430–434 (2017).
12. Deng, F. et al. Hygroscopic porous polymer for sorption-based atmospheric water harvesting. *Adv. Sci.* **9**, 2204724 (2022).
13. LaPotin, A. et al. Dual-stage atmospheric water harvesting device for scalable solar-driven water production. *Joule* **5**, 166–182 (2021).
14. Shan, H. et al. Exceptional water production yield enabled by batch-processed portable water harvester in semi-arid climate. *Nat. Commun.* **13**, 5406 (2022).
15. Song, Y. et al. High-yield solar-driven atmospheric water harvesting of metal–organic-framework-derived nanoporous carbon with fast-diffusion water channels. *Nat. Nanotechnol.* **17**, 857–863 (2022).
16. Wang, J. et al. Water harvesting from the atmosphere in arid areas with manganese dioxide. *Environ. Sci. Technol. Lett.* **7**, 48–53 (2020).
17. Guo, Y. et al. Scalable super hygroscopic polymer films for sustainable moisture harvesting in arid environments. *Nat. Commun.* **13**, 2761 (2022).
18. Fathieh, F. et al. Practical water production from desert air. *Sci. Adv.* **4**, eaat3198 (2018).
19. Hanikel, N. et al. Evolution of water structures in metal–organic frameworks for improved atmospheric water harvesting. *Science* **374**, 454–459 (2021).
20. Zheng, Z., Hanikel, N., Lyu, H. & Yaghi, O. M. Broadly tunable atmospheric water harvesting in multivariate metal-organic frameworks. *J. Am. Chem. Soc.* **144**, 22669–22675 (2022).
21. Kim, H. et al. Adsorption-based atmospheric water harvesting device for arid climates. *Nat. Commun.* **9**, 1191 (2018).
22. Catalanotti, S. et al. The radiative cooling of selective surfaces. *Sol. Energy* **17**, 83–89 (1975).
23. Raman, A. P., Anoma, M. A., Zhu, L., Rephaeli, E. & Fan, S. Passive radiative cooling below ambient air temperature under direct sunlight. *Nature* **515**, 540–544 (2014).
24. Huang, B. L. et al. Thermal conductivity of a metal–organic framework (MOF-5): part II. Measurement. *Int. J. Heat Mass Transfer* **50**, 405–411 (2007).
25. Erickson, K. J. et al. Thin film thermoelectric metal–organic framework with high Seebeck coefficient and low thermal conductivity. *Adv. Mater.* **27**, 3453–3459 (2015).
26. Gunatilleke, W. D. C. B. et al. Thermal conductivity of a perovskite-type metal–organic framework crystal. *Dalton Trans.* **46**, 13342–13344 (2017).
27. Babaei, H. et al. Observation of reduced thermal conductivity in a metal–organic framework due to the presence of adsorbates. *Nat. Commun.* **11**, 4010 (2020).
28. Goswami, A., Pillai, S. C. & McGranaghan, G. Surface modifications to enhance dropwise condensation. *Surf. Interfaces* **25**, 101143 (2021).

29. Donati, M. et al. Dropwise condensation: sprayable thin and robust carbon nanofiber composite coating for extreme jumping dropwise condensation performance. *Adv. Mater. Interfaces* **8**, 2170002 (2021).
30. Cha, H. et al. Dropwise condensation on solid hydrophilic surfaces. *Sci. Adv.* **6**, eaax0746 (2020).
31. Tanner, D. W., Potter, C. J., Pope, D. & West, D. Heat transfer in dropwise condensation—part I the effects of heat flux, steam velocity and non-condensable gas concentration. *Int. J. Heat Mass Transfer* **8**, 419–426 (1965).
32. Hntsberger, J. R. Surface energy, wetting and adhesion. *J. Adhes.* **12**, 3–12 (1981).
33. Zheng, Z. et al. High-yield, green and scalable methods for producing MOF-303 for water harvesting from desert air. *Nat. Protoc.* **18**, 136–156 (2023).
34. Rao, A. K., Fix, A. J., Yang, Y. C. & Warsinger, D. M. Thermodynamic limits of atmospheric water harvesting. *Energy Environ. Sci.* **15**, 4025–4037 (2022).

Acknowledgements

The authors gratefully acknowledge the permission of conducting research in the private property of The Oasis at Death Valley from 22 to 23 August 2022, located in the Furnace Creek, the Death Valley National Park. Z.Z. thanks A. L. Chaudoin from National Park Service for helpful discussion and suggestions on conducting research near the Death Valley National Park area (36.5319° N, −116.5455° W). The authors thank E. Neumann for his help in collecting SEM images and A. Oddo for his engaging educational discussions. This work was supported by the Joint UAEU–UC Berkeley Laboratories for Materials Innovations, the Fifth Generation (W.S. and O.M.Y.), the Defense Advanced Research Projects Agency (DARPA) under contract HR0011-21-C-0020 (W.S., Z.Z., A.H.A. and O.M.Y.) and KACST-UC Berkeley Center of Excellence for Nanomaterials for Clean Energy Applications.

Author contributions

W.S. and O.M.Y. conceived and designed the research. W.S. and O.M.Y. led the project and interpreted the results. W.S. designed, constructed and tested the device. W.S. performed energy transfer simulations. W.S. and Z.Z. synthesized and characterized sorbent samples including powder X-ray diffraction, Fourier-transform infra-red spectroscopy and scanning electron microscopy data. W.S., Z.Z. and A.H.A. performed field test at Death Valley and analysed data. W.S. and O.M.Y. wrote the manuscript, and all the authors reviewed it.

Competing interests

O.M.Y. is co-founder of ATOCO Inc., aiming at commercializing related technologies. The remaining authors declare no competing interests.

Additional information

Supplementary information The online version contains supplementary material available at https://doi.org/10.1038/s44221-023-00103-7.

Correspondence and requests for materials should be addressed to Omar M. Yaghi.

Peer review information *Nature Water* thanks the anonymous reviewers for their contribution to the peer review of this work.

nature portfolio

Corresponding author(s): Omar M. Yaghi

Last updated by author(s): Jun 2, 2023

Reporting Summary

Nature Portfolio wishes to improve the reproducibility of the work that we publish. This form provides structure for consistency and transparency in reporting. For further information on Nature Portfolio policies, see our Editorial Policies and the Editorial Policy Checklist.

Statistics

For all statistical analyses, confirm that the following items are present in the figure legend, table legend, main text, or Methods section.

n/a	Confirmed
☐	☒ The exact sample size (*n*) for each experimental group/condition, given as a discrete number and unit of measurement
☐	☒ A statement on whether measurements were taken from distinct samples or whether the same sample was measured repeatedly
☐	☒ The statistical test(s) used AND whether they are one- or two-sided *Only common tests should be described solely by name; describe more complex techniques in the Methods section.*
☐	☒ A description of all covariates tested
☐	☒ A description of any assumptions or corrections, such as tests of normality and adjustment for multiple comparisons
☐	☒ A full description of the statistical parameters including central tendency (e.g. means) or other basic estimates (e.g. regression coefficient) AND variation (e.g. standard deviation) or associated estimates of uncertainty (e.g. confidence intervals)
☒	☐ For null hypothesis testing, the test statistic (e.g. *F*, *t*, *r*) with confidence intervals, effect sizes, degrees of freedom and *P* value noted *Give P values as exact values whenever suitable.*
☒	☐ For Bayesian analysis, information on the choice of priors and Markov chain Monte Carlo settings
☒	☐ For hierarchical and complex designs, identification of the appropriate level for tests and full reporting of outcomes
☒	☐ Estimates of effect sizes (e.g. Cohen's *d*, Pearson's *r*), indicating how they were calculated

Our web collection on statistics for biologists contains articles on many of the points above.

Software and code

Policy information about availability of computer code

Data collection	All data in this study was collected using commercial softwares including Excel, Origin and LabView.
Data analysis	All data in this study was analyzed using commercial softwares including Excel, Origin and LabView.

For manuscripts utilizing custom algorithms or software that are central to the research but not yet described in published literature, software must be made available to editors and reviewers. We strongly encourage code deposition in a community repository (e.g. GitHub). See the Nature Portfolio guidelines for submitting code & software for further information.

Data

Policy information about availability of data

All manuscripts must include a data availability statement. This statement should provide the following information, where applicable:

- Accession codes, unique identifiers, or web links for publicly available datasets
- A description of any restrictions on data availability
- For clinical datasets or third party data, please ensure that the statement adheres to our policy

The data sets that support this study are available in Zenodo repository with identifier (http://doi.org/10.5281/zenodo.7990951).

Human research participants

Policy information about studies involving human research participants and Sex and Gender in Research.

Reporting on sex and gender	No sex and gender related information has been collected in this study.
Population characteristics	No human participants were involved in this study.
Recruitment	No human participants were involved in this study.
Ethics oversight	No approval was needed for this study.

Note that full information on the approval of the study protocol must also be provided in the manuscript.

Field-specific reporting

Please select the one below that is the best fit for your research. If you are not sure, read the appropriate sections before making your selection.

☒ Life sciences ☐ Behavioural & social sciences ☐ Ecological, evolutionary & environmental sciences

For a reference copy of the document with all sections, see nature.com/documents/nr-reporting-summary-flat.pdf

Life sciences study design

All studies must disclose on these points even when the disclosure is negative.

Sample size	Not applicable for this study.
Data exclusions	Not applicable for this study.
Replication	Not applicable for this study.
Randomization	Not applicable for this study.
Blinding	Not applicable for this study.

Reporting for specific materials, systems and methods

We require information from authors about some types of materials, experimental systems and methods used in many studies. Here, indicate whether each material, system or method listed is relevant to your study. If you are not sure if a list item applies to your research, read the appropriate section before selecting a response.

Materials & experimental systems

n/a	Involved in the study
☒	☐ Antibodies
☒	☐ Eukaryotic cell lines
☒	☐ Palaeontology and archaeology
☒	☐ Animals and other organisms
☒	☐ Clinical data
☒	☐ Dual use research of concern

Methods

n/a	Involved in the study
☒	☐ ChIP-seq
☒	☐ Flow cytometry
☒	☐ MRI-based neuroimaging